Aero-thermo-chemical characterization of Ultra-High-Temperature Ceramics for aerospace applications

Raffaele Savino, Luigi Criscuolo, Giuseppe Daniele Di Martino, Stefano Mungiguerra*

University of Naples "Federico II"

Department of Industrial Engineering-Aerospace Section,

80 P. le V. Tecchio, Naples, Italy 80125

Abstract

Ultra-High-Temperature Ceramic (UHTC) materials, because of their high temperature resistance, are suitable as thermal protection systems for re-entry vehicles or components for space propulsion. Massive UHTC materials are characterized by poor thermal shock resistance, which may be overcome using C or SiC fibers in a UHTC matrix (UHTCMC).

The University of Naples "Federico II" has a proven experience in the field of material characterization in high-enthalpy environments. A hypersonic arc-jet facility allows performing tests in simulated atmospheric re-entry conditions. The Aerospace Propulsion Laboratory is employed for testing rocket components in a representative combustion environment. Ad-hoc computational models are developed to characterize the flow field in both facilities and perform thermal analysis of solid samples.

Current research programs are related to a new-class of UHTCMC materials, for rocket nozzles and thermal protection systems. The activities include design of the prototypes for the test campaign, numerical simulations and materials characterizations.

Keywords: Ultra-High-Temperature Ceramic Matrix Composites; Arc-jet experimentation; Rocket nozzles; Numerical simulations

1 Introduction

Ultra-High-Temperature Ceramic (UHTC) materials are assuming an increasing importance in aerospace research because their high temperature capabilities make them interesting to develop components for extreme applications, such as thermal protection systems of hypersonic or atmospheric reusable re-entry vehicles, specific components for propulsion, combustion chambers, engine intakes or rocket nozzles [1-4]. Indeed, UHTC materials are characterized by unique combination of properties, including melting points above 3500 K, high temperature strength and capability to manage and conduct heat when the service temperatures exceed 2200 K [1]. These characteristics allow UHTCs to work in thermo-chemically aggressive environments encountered in the most demanding space applications [4-8]. During hypersonic re-entry, shock waves in front of the nose tip and of the wing leading edges of the spacecraft cause the temperature to rise up to thousands of Celsius degrees, activating also gas dissociation/recombination reactions. On the other side, rocket nozzles, having the function to expand high enthalpy reacting gases, coming from the combustion chamber, are subject to chemical and mechanical erosion in presence of high pressures, in the order of tens of bars, and flame temperatures higher than 3000 K. At present, the structural materials for use in aerospace high temperature oxidizing environments are limited to Silicon-based ceramics (e.g. SiC) and protected C/C composites, with maximum service temperature up to ~2000 K [9,10].

* Corresponding author.
E-mail address: s.mungiguerra@studenti.unina.it

UHTC materials generally include transition metal diborides and transition metal carbides (i.e. ZrB_2, HfB_2, ZrC, HfC, TaC). The use of single phase materials, without secondary phases, is not sufficient for extreme applications because these materials are vulnerable to oxidation attack, characterized by low fracture toughness, low thermal shock resistance and lack of damage tolerance, therefore they are unacceptable for aerospace engineering applications. To improve properties, UHTCs composites with SiC or other Silicon based ceramics, in the form of particles, short fibers and whiskers have been developed with better tolerance and thermal shock resistance in aggressive chemical environments [11,12]. Unfortunately, despite the very good oxidation resistance of small specimens, larger UHTC components frequently exhibited poor reliability and were subject to failures in high enthalpy flows. On the basis of these results, the current research activities are oriented towards Ultra-High-Temperature Ceramic Matrix Composites (UHTCMC) materials based on C or SiC fibers in UHTC matrices, that represent the next step to introduce significant improvements in comparison to the state-of-art materials for aerospace applications.

One of the most important features of ceramic materials for TPS applications is the resistance to oxidation/ ablation, which can be investigated by flight experiments or simulated in ground based experiments with hypersonic wind tunnel facilities. The most significant tests to study the materials behavior in a relevant environment with ground based simulation experiments are carried out in arc-jet hypersonic plasma wind tunnels [13,14]. For materials screening purposes, sometimes also other techniques can be used like high power laser beams [15], plasma or oxyacetylene torch [16-18] which can provide conditions of intense heat fluxes and ultra high temperatures. They are therefore convenient especially for primary qualitative evaluation of the thermal shock resistance and ablation resistance properties of different materials. Also, materials for rocket components can be tested by means of similar low-cost techniques [19,20], but the most relevant thermo-fluid-chemical environment can only be reproduced in dedicated rocket propulsion facilities.

The University of Naples “Federico II” has a proven experience in aero-thermo-dynamics and rocket propulsion research, including characterization of materials in extreme aerospace environments. Many studies have been published on UHTC characterization in simulated hypersonic re-entry conditions [21-24]. More recently, the propulsion laboratory with a dedicated hybrid rocket engine has been dedicated to specific tests on different nozzles materials under severe operating conditions [19,25].

This article is an overview of the main research activities performed so far, as well as an introduction to the current programs including UHTC characterization in both propulsion and atmospheric reentry environments, in the framework of the European Project C^3HARME – Next Generation Ceramic Composites for Combustion Harsh Environment and Space.

2 Aerothermodynamics

Research activities in the Aerospace section of the University of Naples “Federico II” include high speed aerodynamics, aerothermochemistry, propulsion, system configuration design, laboratory experiments and verification, flight experimentation. Relevant contributions have been focused on advanced winged reentry spaceplanes [26], high speed aircrafts for space tourism [27,28], numerical and experimental studies in the frame of the IXV (Intermediate Experimental Vehicle) ESA program [29]. The research group is presently also involved in programs dedicated to the development of deployable re-entry capsules [30-33].

Many applications, such as high-lift re-entry vehicles with sharp wing leading edges or new hybrid rockets require advanced materials able to withstand relevant thermo-mechanical loads in aggressive chemical environments. For these applications, UHTC materials are studied using a hypersonic arc-jet plasma facility, able to simulate supersonic atmospheric re-entry conditions, and a lab-scaled hybrid rocket available in the propulsion laboratory. These facilities, the experimental set up, the theoretical and numerical models for correlation and better interpretation of the experimental results will be presented and discussed.

2.1 Hypersonic arc-jet facility

The Small Planetary Entry Simulator (SPES) facility available for the simulation of atmospheric re-entry flows (Figure 1) is a continuous, open-circuit, blow-down arc-jet wind tunnel. The plasma is generated by an industrial torch with maximum power of 80 kW, able to operate with inert gas (He, N_2, Ar and their mixtures) at mass flow rates up to 5 g/s. Specific total enthalpies above 20 MJ/kg are achieved at gas mass flow rate of 1 g/s. In order to simulate the air composition, a mixer downstream the torch is used to supply a secondary gas (e.g. O_2) to the primary nitrogen plasma. Converging–diverging nozzles with different area ratios accelerate the high enthalpy flow to a nominal Mach number in the range 3-5. The specimen in the test chamber can be analyzed thanks to infrared and optical windows.

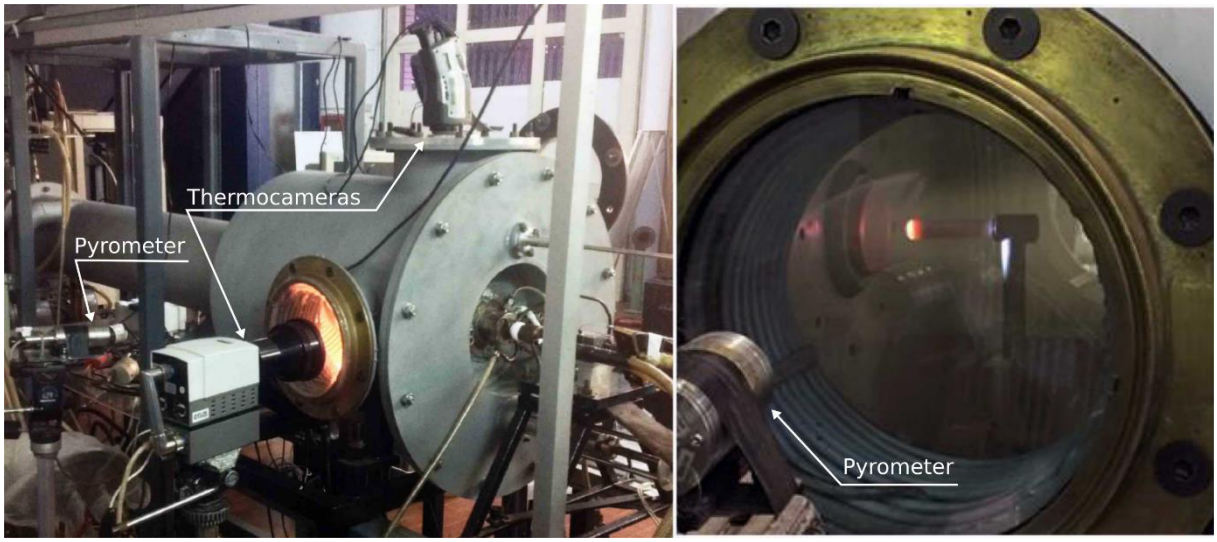

Figure 1 Arc-heated facility available at the University of Naples.

A combination of direct and alternate voltage provided by electrodes and a radiofrequency starter (2 kV at 1 MHz) is used to trigger the arc heater. An electric system allows to control and regulate the mass flow rate and the torch power. The specific total enthalpy is estimated at the exit of the torch and at nozzle exit by means of an energy balance. The main parameters to simulate supersonic high enthalpy conditions include the gas mixture composition and its flow rate, the pressure distribution onto the specimen's surface, the total enthalpy and the surface heat flux. A two-color pyrometer and a thermocamera are available for non-intrusive temperature measurements (see Figure 1).

2.2 Aerothermodynamic characterization of UHTC

The arc-jet facility has been utilized to test specimens with different shapes and sizes in a relevant atmospheric re-entry environment. Tests are typically performed increasing the total enthalpy of the flow with several steps, corresponding to increasing torch arc power, leading correspondingly to an increase of the temperature and pressure (Figure 2). Figure 2 shows a qualitative time profile of the surface temperature detected by the infrared instruments, while Table 1 shows typical values for a test with 5 steps and total duration of about 5 minutes, when the mass flow rate is 1 g/s. In general, when the maximum total enthalpy is established, a quasi-constant, maximum value of the temperature is reached.

	STEP 1	**STEP 2**	**STEP 3**	**STEP 4**	**STEP 5**
Arc current [A]	300	400	500	600	650
Arc power [kW]	16	22	29	37	41
Specific enthalpy [MJ/kg]	8	11	14	19	21
Stagnation pressure [Pa]	7500	8500	9500	11000	11500

Table 1 Typical parameters in an arc-jet test, 1 g/s of air flow rate.

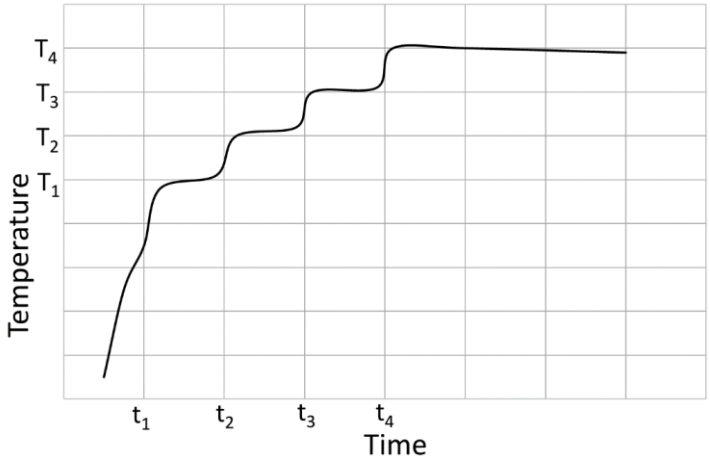

Figure 2 Typical qualitative temperature trend in SPES experimentation.

Table 2 summarizes the typical test conditions for experimentation in SPES wind tunnel. As explained above, they are referred to a mass flow rate condition of 1 g/s.

Test duration	1 – 10 min
Max Specimen Temperature	>2000 K
Max Total Specific Enthalpy	> 20 MJ/kg
Max Flow Temperature	5000 – 6000 K
Max wall total heat flux	> 10 MW/m^2

Table 2 Typical operative and environmental conditions in a SPES test.

The actual value of the heat flux on the specimen is strongly influenced by the material properties, as discussed in Section 2.3. The test articles can be accommodated inside the test chamber of the plasma wind tunnel, at the exit of the supersonic nozzle, by using a dedicated set-up with thermally protected mechanical supports (Figure 1,Figure 4), the position can be regulated to place the sample at the desired distance from the nozzle.

In previous research activities, samples with different shapes have been tested in SPES arc-jet facility, in order to simulate the conditions reached at the stagnation point of a re-entry vehicle, with flat or hemispherical specimens, or on leading edges, with the wedge shape. Typical sizes of the samples are in the order of 1 cm. Figure 3 shows samples of different shapes, sizes, made of different UHTC compositions, tested in the arc-jet facility during different research campaigns.

Figure 4 shows a typical experimental setup in arc-jet facility, the picture is related to the research activities on thermo-chemical surface instabilities of SiC-ZrB_2 ceramics in high enthalpy dissociated supersonic air flows. The test article is a cylindrical flat sample with button-like shape as illustrated in Figure 3 (1a). The surface temperature of the sample was continuously measured (±1% accuracy) by a digital two-color pyrometer (Infratherm ISQ5, Impac Electronic GmbH, Germany) at an acquisition rate of 100 Hz. The measurement area of the optical pyrometer was approximately a round spot 3.3 mm in diameter, Figure 5. The surface temperatures of the samples were experimentally determined coupling the infrared thermo-camera to the optical pyrometer.

Figure 3 (1b) shows the cylindrical flat sample after the test under supersonic high enthalpy conditions. Figure 6 shows a Scanning Electron Microscopy (SEM) micrograph of the UHTC article after the test to highlight the typical behavior of the material under simulated atmospheric re-entry conditions. The microstructures of the UHTC sample is characterized by a layered multiphase configurations of catalytic oxide scale (mixed ZrO_2/glass), and an unoxidized band some tenths of micron thick.

Figure 7 shows the very sharp wedge of Figure 3 (3a) made of ZrB_2-SiC during exposition to the supersonic plasma. This test article was compared with a sample with the same sharp shape made in lower thermal conductivity ceramic material (Si_3N_4–$MoSi_2$) [22].

When subjected to heat fluxes in the order of 7 MW/m^2, the surface temperature of the UHTC wedge increased up to 2700 K near the leading edge. The highly thermally conductive UHTC survived such extreme conditions by re-distributing heat over colder regions downstream of the sharp tip. As a consequence, radiative equilibrium temperatures in the range 1700-2000 K were established over 85% of the exposed surface. On the other hand, the less thermally conductive Si_3N_4–$MoSi_2$ material failed to withstand the same heat flux and underwent partial melting with significant mass loss. Figure 8 shows the sharp wedge models after the experimental campaign in SPES arc-jet facility, and demonstrates the previous considerations about the UHTC.

Another example is the asymmetrical leading edge demonstrator of Figure 3 (4a), made of ZrB_2–SiC, which has been designed with the aim to analyze the response to heat flux conditions typical of thermal protection systems of re-entry spacecrafts [21]. The sample was manufactured and tested under a non-equilibrium supersonic airflow of 21 MJ/kg total enthalpy. The length is 1 centimeter. Figure 3 (4c) shows the sharp leading edge during the test. The ultra-refractory sample withstood stressful thermo-chemical loads successfully, without obvious failure. Figure 3 (4b) shows the sample after the test campaign. From that picture the in-situ formed oxide scale is evident in light grey near the tip of the leading edge.

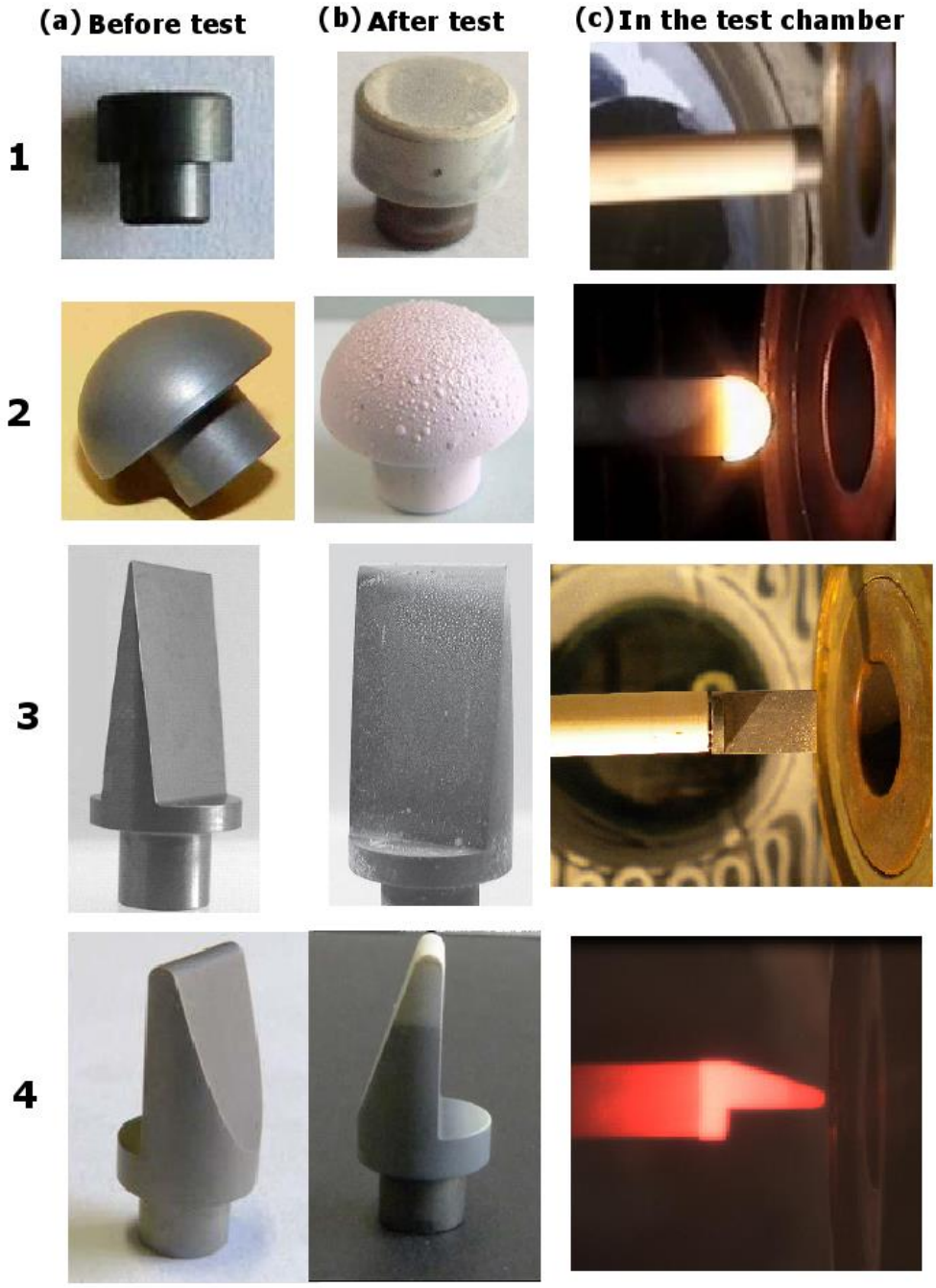

Figure 3 (1) Flat cylinder sample (button- like shape) [34], (2) hemispherical sample [35-38], (3) symmetrical sharp leading edge [22,39], (4) asymmetrical sharp leading edge [21].

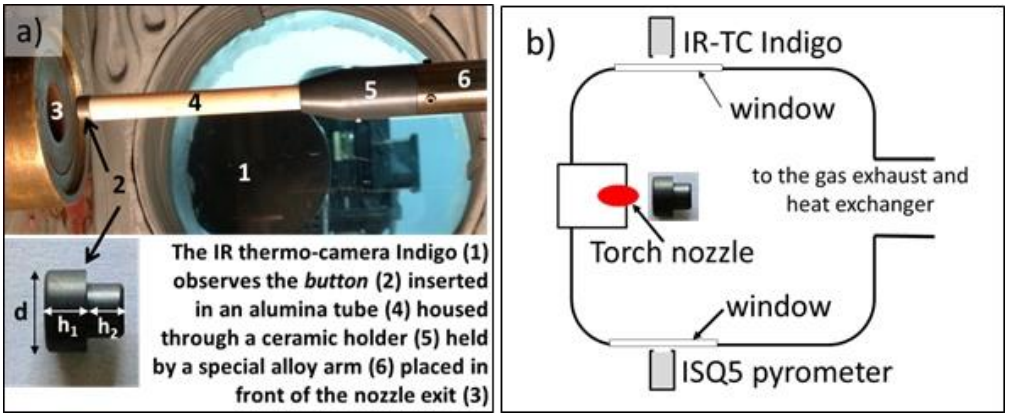

Figure 4 Experimental set-up inside the testing chamber during arc-jet. The inset shows a virgin cylindrical flat sample: h_1= 5 mm, h_2= 5 mm, and d=10 mm as diameter [34].

Figure 5 Time-resolved onset of the bow-shock during the early stages of aero-heating: the arbitrary sequence of CCD frames is phased (2 s full duration). The red full circle locates the measurement area of the two-color ISQ5 pyrometer. The lateral perimeter of the button is outlined [34].

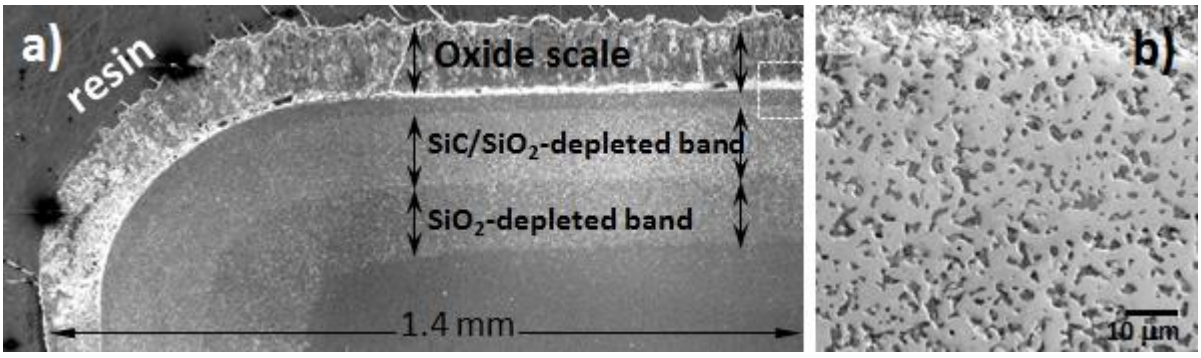

Figure 6 The layered multiphase configuration of the oxidized scale microstructures (a, SEM micrograph) of the ZSW button after ZSW-1 test. The white box in a), expanded in b), highlights an unoxidized band, some tenths of micron thick, sandwiched between the mixed ZrO_2/glass scale and the$SiC+SiO_2$ depleted bands [34].

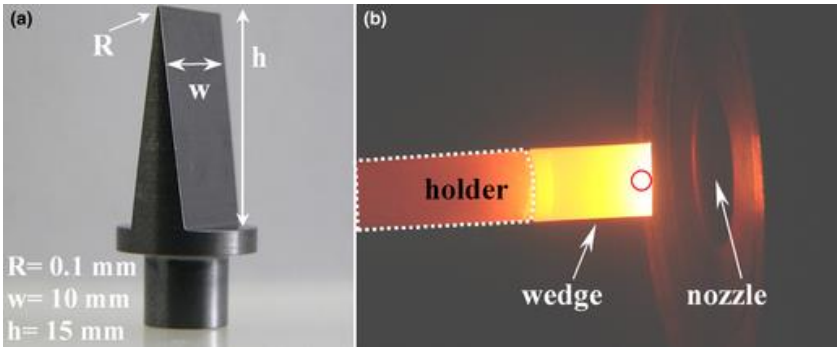

Figure 7 The ZrB_2 – SiC wedge, R radius of curvature: (a) as-machined, (b) inside the arc-jet camera; circle: position and size of the pyrometer's spot recording temperature during testing [22].

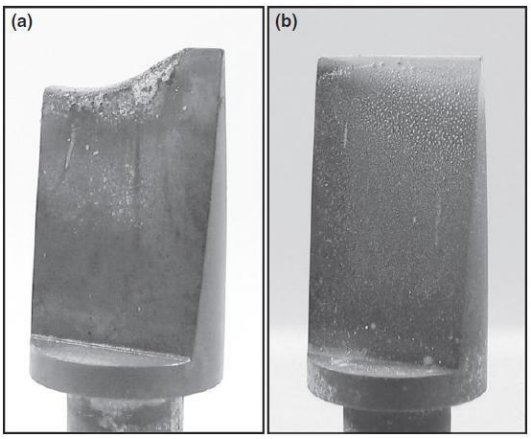

Figure 8 Sharp wedge models after the tests in SPES arc jet facility: (a) the Si_3N_4–$MoSi_2$ wedge after one test, (b) the ZrB_2 – SiC wedge after two consecutive tests [22].

As discussed later on, the representative aero-thermo-chemical conditions occurring when the test article is exposed to the high enthalpy chemically reacting supersonic flow can be numerically simulated with state of art computational fluid dynamics codes. One of the aims is to evaluate the different contributions to the heat flux resulting in the final thermal equilibrium conditions. For instance, as shown in Figure 9, when a relatively sharp leading edge sample is exposed to the high enthalpy supersonic flow (the shock wave is highlighted), the convective heat flux entering the surfaces is partly transferred away through the solid and partly re-radiated back to the environment. Since a steady state is achieved, global radiative equilibrium is established, in the sense that the overall surface convective heat flux is balanced by the overall surface radiative heat flux and by the conduction heat transfer.

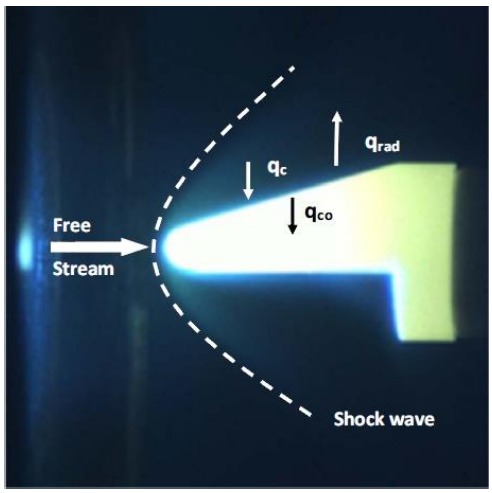

Figure 9 UHTC Leading edge during the test: the convective heat flux (q_C) is partly transferred by conduction (q_{CO}) and re-radiated to the environment (q_{RAD}) [21].

2.2.1 Further considerations on arc-jet testing and other characterization techniques

As explained in the Introduction, arc-jet plasma wind tunnels are the facilities in which the most relevant environment can be reproduced when testing various materials. Other techniques, such as laser beams, plasma or oxyacetylene torches, allow a preliminary screening of the materials in representative conditions of heat flux and temperature.

A hypersonic wind tunnel can additionally provide the real gas flow conditions and shear stresses at the realistic static and dynamic pressures to simulate real flight environments and related fluid-solid surface interactions. The main difference, in comparison to the aforementioned relatively less expensive techniques, is related to the gas composition and to the aero-thermodynamic (gas flow) conditions. An air plasma may exhibit very high temperatures (in excess of 5000 K) and Mach number in excess of 3 with highly dissociated gas species (oxygen and nitrogen). On the other hand, oxyacetylene torch produces a confined jet of combustion products (carbon mono/dioxide, water vapor, OH and active hydrocarbon species) at lower (subsonic) Mach number and temperatures in the order of 3000 K. The specific total enthalpies are relatively lower than in typical atmospheric reentry conditions.

When testing C/C, C/SiC or UHTC ceramic composites, some inconsistent or even contradictory results were reported in the literature [40]. For instance, it was reported that C/C composites and UHTC composites (C/C-ZrC composites and C/C-ZrC-SiC composites) exposed to the same oxyacetylene torch under the same conditions for the same time (20 s), exhibited very similar linear ablation rates (0.012-0.013 mm/s). However, for the different materials, the ablation rate is strongly dependent on the exposition time. For instance, for the C/C-ZrC composites, it is strongly decreasing when the exposition time increases from 20 s to 50 s. Furthermore, another C/C-ZrC-SiC composite fabricated with the same process exhibited an ablation rate of 0.002 mm/s.

On the other hand, the C/C-ZrC-SiC composites, when exposed to an arc-jet hypersonic wind tunnel at similar heat fluxes and temperatures (from 2000 K to 2500 K) for a prolonged time of 600 s exhibited an ablation rate of 0.0016 mm/s.

The flame torch operates at subsonic flow conditions and atmospheric pressure. Therefore the ablation is generally induced by oxidation and vaporization with weak effects of surface shear stresses. Whereas, in hypersonic reentry flow or in supersonic flows in nozzles of rockets, ablation is additionally enhanced by high-velocity-induced mechanical erosion.

Another important difference is related to the different surface modifications occurring in different gas environments, even if heat fluxes and temperatures are comparable. Previous experiences [37] showed that the same UHTC materials, exposed for prolonged time to the plasma torch and to supersonic arc-jet streams of simulated air composition, underwent different surface modifications, as confirmed by post inspections with microscopic analyses. The materials behavior, after exposition to the plasma torch at surface temperatures in the order of 2000 K, was different, and this could be explained by the different pressures and shear stresses and by the different degree of dissociation of the chemical species in the different testing conditions. The different macroscopic result was a different emissivity, as measured with the same two color pyrometer and infrared thermocamera in the two experiments. In the plasma torch experiments corresponding to high enthalpy subsonic flow conditions (atmospheric pressure discharge) the surface emissivity is 0.9 while in supersonic arc-jet experiments the emissivity is lower (0.7 at the highest temperature). This shows that the surface oxidation is affected not only by the total enthalpy level of the flow but also by the peculiar flow behavior and that in hypersonic conditions the material response can be greatly different. Larger leading edges models of UHTC materials, fabricated with the same ceramic (ZrB_2-SiC) compositions and with the same hot pressing process at the Institute of Science and Technology for Ceramics (ISTEC), were tested in a hypersonic plasma wind tunnel facility at German Aerospace Center (DLR) under comparable conditions in terms of total enthalpy and stagnation point pressure, reaching lower

temperatures (in the order of 1800 K) due to the larger curvature radius. However, the numerical model, integrated with the values of the emissivities measured on small samples of the same material, was able to well correlate also in this case the thermal evolution, experimentally evaluated with an infrared camera operating at the same wavelength band of the previous one. The estimated surface catalytic atomic recombination efficiency decreased with the temperature, from values in the order of 0.1 at temperatures up to 800 K to 10^{-4}, at temperatures > 1200 K.

To further support these considerations, in [41], ZrB_2-SiC ceramic samples were exposed to a subsonic plasma jet, at atmospheric pressure. Total enthalpies higher than 10 MJ/kg were reached, for a maximum wall heat flux of 7 MW/m^2, corresponding to a maximum temperature of 2200 K. SEM analyses performed after the test showed the formation of a glassy layer, protecting the external surface directly facing the oxidizing environment (Figure 10 (a)).

On the other hand, the characterization of samples with the same composition in arc-jet facility, with supersonic flow and low partial pressure (in the order of some kPa) conditions resulted in a different material surface behavior [34]. In this case, although lower heat fluxes (3.5 MW/m^2) and maximum temperatures (2000 K) were reached (but with a specific total enthalpy of 18 MJ/kg), the coating was wiped away and the oxidation proceeds faster, leaving a more catalytic oxide scale (Figure 10 (b)).

This demonstrates once more that, even reproducing the same chemical environment, the material's response is significantly influenced by the operating conditions.

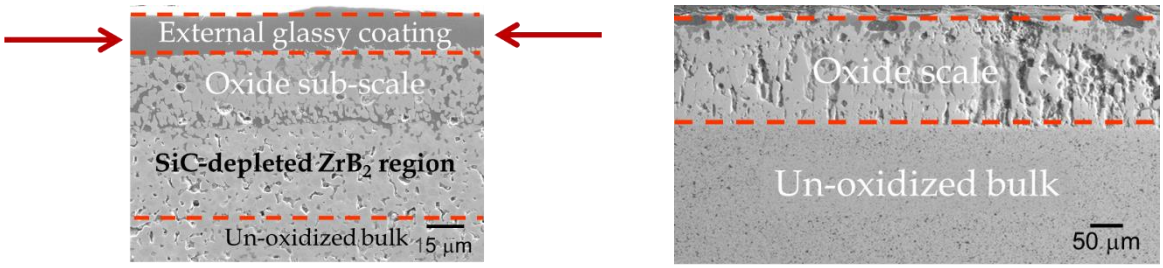

(a) (b)

Figure 10 Cross-section of a ZrB_2–15SiC material (a) after subsonic plasma torch testing (at atmospheric pressure) [41] and (b) after supersonic arc-jet testing (at low pressure) [34].

Another important example of the effect of peculiar test conditions on material surface modifications is the spontaneous temperature jump phenomenon reported by Marschall [42] and then found also by other authors [43]. When a sample of material in presence of Si-containing compounds is exposed to a flow of constant total enthalpy for some minutes, the surface temperature after having reached an apparent steady state exhibits an abrupt jump of several hundreds of degrees due to the change of the surface properties (like emissivity or catalycity) that may lead to a completely different surface heat flux, under the same free stream conditions.

The conclusion is that when UHTC materials are characterized with plasma or oxyacetylene torches or even with other heating systems in gas environments that are not properly reproducing the gas composition, pressure and shear conditions, different surface modifications are possible and these may alter important surface properties like emissivity and catalycity. This means that even if the heat flux is the same, the materials response may be very different, compared to what happens in real flight environment.

This should be taken into account in future characterization and qualification of materials in real relevant environments.

2.3 Numerical models and simulations

As explained in Section 2.2, in order to support the experimental activities, numerical models were developed to predict the flow field in the facility and the thermal behaviour of the samples.

A one-dimensional model, based on NASA CEA (Chemical Equilibrium with Applications) software [44], can be used to predict the flow field in the facility nozzle. The evolution of high-enthalpy molecular gases (e.g. N_2, O_2) is simulated through the nozzle, in the assumption of frozen equilibrium in the divergent part. A mass balance is used to evaluate the pressure upstream the nozzle (i.e. in the mixing chamber, in blue in Figure 11). The outputs of the simulations are the fluid dynamic conditions and the chemical composition at the nozzle exit, i.e. at the inlet of the test chamber. These values can be used as inputs for computational fluid dynamic (CFD) simulations of the test chamber.

CFD is also often used to evaluate the flow conditions in the facility. Both 2-D axisymmetric and 3-D computational domains can be used to simulate steady and unsteady flows. An example mesh for CFD analyses is shown in Figure 11, representing the main elements of the facility, including the test chamber. Figure 11 also highlights the sections in which N_2 and O_2 are injected. Chemical non-equilibrium models with at least five reacting species (N_2, N, O_2, O, NO) are implemented to describe the chemical field, involving dissociation reactions. In case of more than five species, also ionization is taken into account. Turbulence/chemistry interaction models can be considered to describe properly the temperature and species distribution.

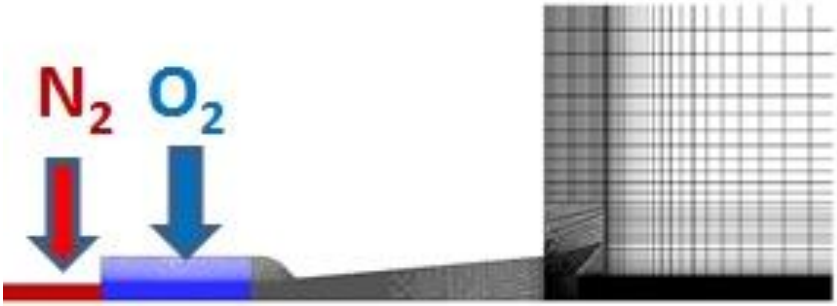

Figure 11 Typical CFD grid for SPES simulation [34].

Figure 12 shows an example of Mach number contour obtained by means of CFD simulations, for an arc power of 29 kW: it is possible to see that the Mach number is 3 at nozzle exit.

The thermo-fluid-dynamic conditions achieved at nozzle exit by means of CFD simulations or, as anticipated above, calculations via CEA software, can be then used as boundary conditions to reproduce the flow-field surrounding the sample.

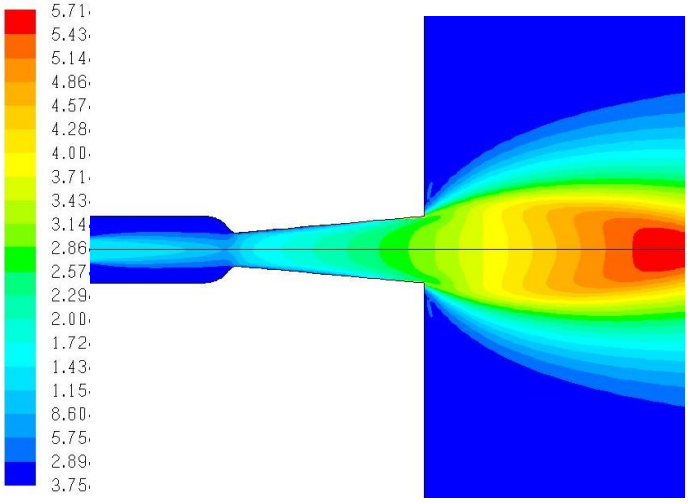

Figure 12 Mach number contours inside SPES nozzle and test calculated by means of CFD [37].

Finally, thermal analyses of the samples can be performed. Two different approaches can be adopted:

- decoupling the flow field from the thermal field inside the material;
- considering the fluid/material interaction for a more accurate analysis.

An example of CFD grid used for thermal analyses on a button-like ZrB_2-SiC specimen, with a radius of 5 mm, is shown in Figure 13 [34]. In particular, on the left, the computational domain used to calculate the thermal field inside the solid specimen and its ceramic supporting tube is shown; on the right, there is a zoom on the mesh of the flow around the test article. The numerical simulations were performed for comparison with the experimental results obtained in the parallel test campaign.

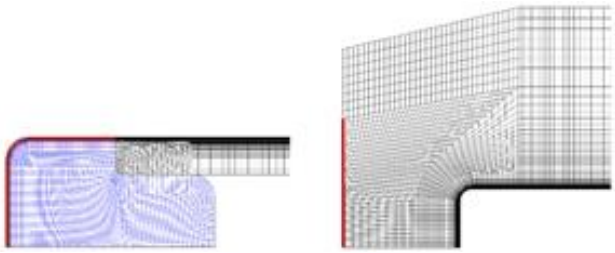

Figure 13 Computational grids used for thermal analyses on ZrB_2-SiC button-like samples [34].

CFD simulations performed on the grid shown on the right in Figure 13 allowed to describe the thermo-fluid-dynamic conditions around the sample and to evaluate the heat flux on the surface of the specimen. A steady-state simulation was performed, assuming an average total enthalpy of the flow of 21 MJ/kg (corresponding to the conditions achieved during a test), a surface emissivity ε = 0.7 and a catalytic efficiency γ = 0.01. Figure 14 shows the static pressure and the temperature around a sample computed by CFD analysis. The different components of the heat flux calculated are shown in Figure 15, together with the profile obtained under the hypotheses of cold and not catalytic wall.

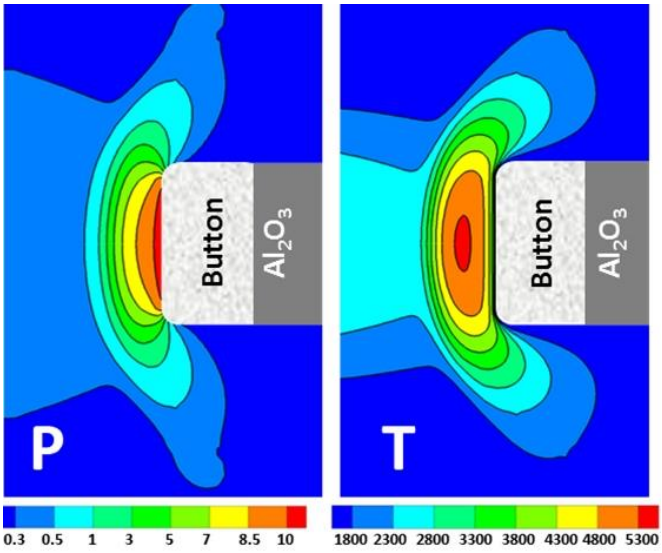

Figure 14 Static pressure P_{STAT} (Pa) and temperature T_{STAT} (K) around the flat cylinder sample computed by CFD analysis [34].

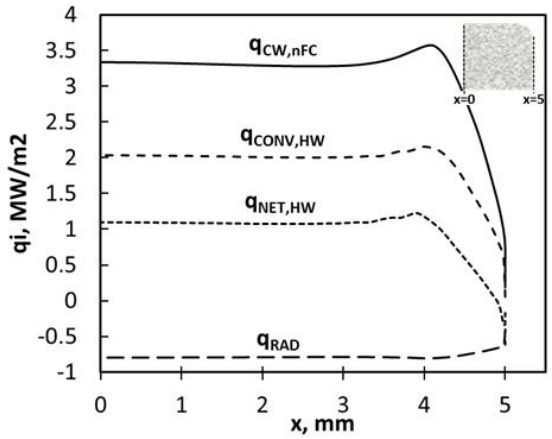

Figure 15 Various components of the heat flux (qi) vs x coordinate of the sample computed by CFD analysis for H_0=21 MJ/kg, ε_T=0.7 and γ=0.01: hot-wall convective (CONV, HW), radiative (RAD) and net hot-wall (NET, HW). The initial cold-wall zero-catalytic heat flux was also calculated (i.e. γ=0, CW, nFC) [34].

The numerical results of the heat fluxes were then used to calculate the temperature field inside the material sample. Figure 16 compares the values of surface temperature obtained by means of CFD, with the computational grid shown on the left in Figure 13, and the ones measured, by means of an infrared thermocamera, during the test in reference [34]. The temperature was evaluated along the black dashed line shown in Figure 16b. The CFD outputs provided a robust sketch of how steep can be the surface temperature increment along the exposed flat surface to the hot plasma of the button.

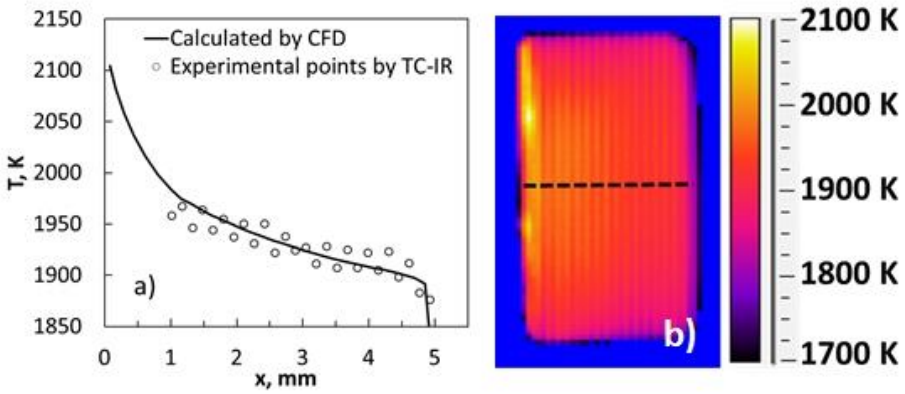

Figure 16 Comparison between numerical and experimental evaluations of the surface temperature on a SiC-ZrB_2 cylindrical sample during a test in [34].

During the test in arc-jet [34], two special events were detected and identified, the *hot-spots* and the *waves of radiance,* both directly associable to transient thermo-chemical instabilities of the in-situ changing oxide scale under severe aero-thermal heating. The *hot-spots* are anomalous and spatially resolved enhancements of the emitted spectral radiance. The *waves of radiance* draw colored bands, regularly moving in the same direction of the gas stream, real time recorded by a IR-thermocamera during the most stressful stages of the thermal history.

The sensitivity of the thermal field to the surface properties was also evaluated. As anticipated in Section 2.1, heat flux and surface temperature are consistently influenced by catalytic efficiency and surface emissivity. Values of catalytic efficiency γ in the order of 0.1 can lead to an increase in the specimen temperature up to 500 K.

3 Rockets Propulsion

3.1 Hybrid rocket Laboratory

The Aerospace Propulsion Laboratory of the University of Naples "Federico II" was set up primarily for the purpose of testing hybrid rocket engines. Being equipped with a test bench and a general purpose acquisition system, it is versatile as it is possible to easily adjust the experimental apparatus to several classes of tests, including evaluation of performances of propellants and combustion processes, testing of sub-components and/or complete power systems, nozzles, catalytic systems, burners, ignition and cooling systems.

A picture of the 200-N class rocket engine during a typical test in the laboratory is shown in Figure 17.

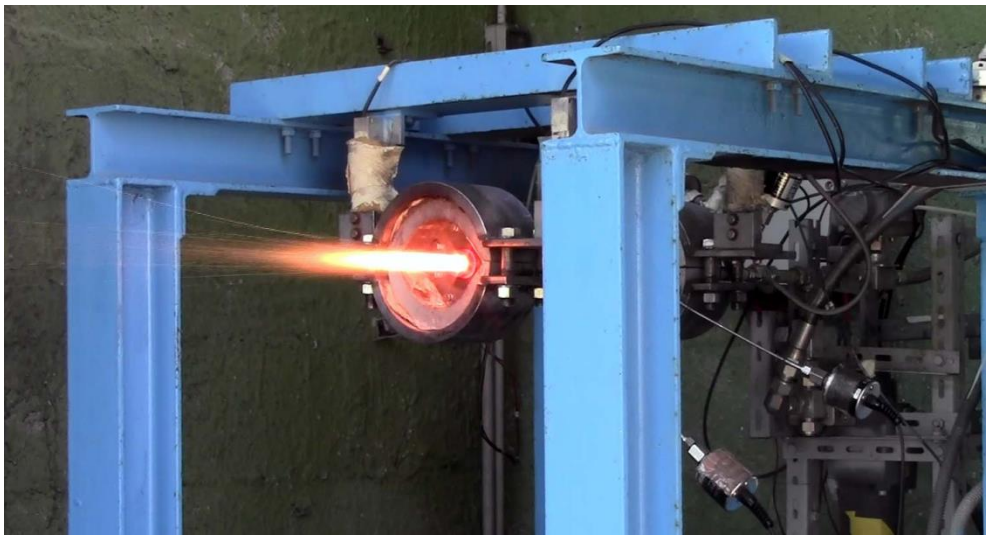

Figure 17 Lab scale hybrid rocket available at Aerospace Propulsion Laboratory of the University of Naples.

Different oxidizers (e.g. oxygen or nitrous oxide) can be stored in tanks and supplied to the motor with a feed line regulated electronically with a controlled pressure valve. The mass flow rate is evaluated measuring the gas temperature and pressure upstream of the throat of a chocked Venturi tube. Nitrogen is purged into the chamber for burn-out or in case of unexpected phenomena.

The lab-scale rocket has an axisymmetric combustion chamber, with 350-mm length and 70-mm inner case diameter. The motor forward closure can accommodate different injectors, such as, for instance, axial nozzle, showerhead and axi-radial. Upstream and downstream of the solid grain a dump plenum and an aft-mixing chamber are set up, respectively. The pre-chamber shifts towards the fore end of the grain the broad oxidizer recirculation, in order to increase the overall regression rate. The post-chamber in stainless steel, thermally insulated, as usually required in hybrids, promotes gas mixing at the exit of the fuel port, thereby improving combustion efficiency. Graphite converging-diverging nozzles with 10 mm throat diameter are usually employed, but it can be easily replaced by segmented nozzles with UHTC (or other materials) throat insert or by complete ceramic nozzles.

The motor is supported on the test bench with 4 load cells; this assembly allows evaluating the motor thrust by measuring the forces within each cell. The combustion pressure is measured by capacitive transducers set up in the pre-chamber and in the aft-mixing chamber.

A spark plug powered by a Honeywell solid-state igniter spark generator is arranged in the pre-chamber, where methane gas is injected for few seconds simultaneously with the oxygen to ignite the motor. This system ensures repeatable ignition conditions as well as motor re-ignition.

The analog signals generated by thermocouples, pressure transducers and load cells are sampled at 5 kHz, digitally converted, processed and recorded on the hard disk by a PXI Express standard system interconnected with the computer by means of optical fibers connections. With this equipment and using a software developed in LabView, the motor is ignited and the firing test is completely automated.

3.2 Ceramic nozzles characterization

An experimental set up was prepared for characterization of composite ceramic materials under extreme conditions representative of a propulsion environment [25]. The nozzle was a segmented converging/diverging (de Laval) nozzle allowing to insert a throat fabricated with a UHTC ceramic material. A Tantalum Carbide (TaC)-based material was manufactured by ISTEC and tested in the lab scaled hybrid rocket engine for comparison with a similar graphite nozzle insert.

TaC is a strong and stiff material and its thermal conductivity shows the tendency to increase with increasing the temperature at least in the range tested [45]. The linear coefficient of thermal expansion (CTE) is similar to other transition metal carbides. The fracture toughness associated to the stiffness is the reason for the poor thermal shock resistance, that is however, not notably different from those of other UHTC ceramics [46].

Two tests were carried out at the same experimental conditions, with different nozzles. In both cases the segmented nozzles have converging and diverging elements in graphite but the throat insert is again in graphite or in TaC-based composite material.

The nozzle dimensions are shown in Figure 18. Figure 19 shows some pictures of the components of the segmented nozzle with the TaC-based throat section and the converging and diverging parts made in graphite. The ceramic composite had the following composition: TaC + 10 vol% $MoSi_2$; it was produced starting from commercial raw materials.

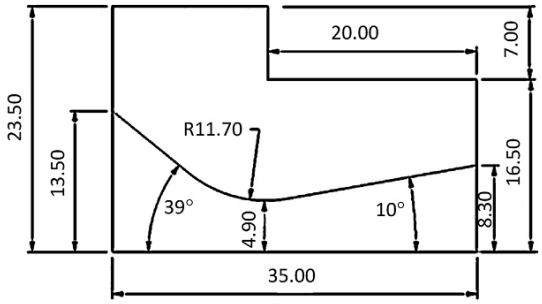

Figure 18 Layout De Laval nozzle geometry (dimensions in millimiters).

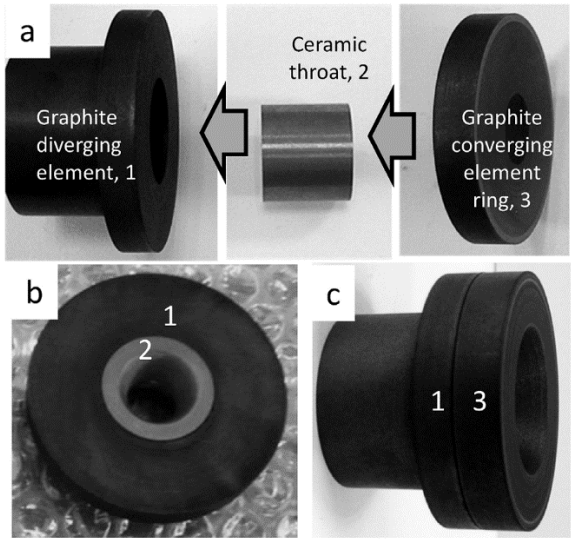

Figure 19 (a) Segmented nozzle, composed of a graphite diverging element (1), ceramic throat made of TaC-based composite material (2), and outer graphite converging element (3). (b) Ceramic throat inserted into the graphite body, (c) complete nozzle assembly [25].

Gaseous oxygen was used as oxidizer and High-Density PolyEthylene was used as a fuel. The oxidizer mass flow rate was kept to a constant value of 27 g/s for 10 s. The fuel grain had a simple cylindrical port.

Figure 20 shows the time history of the pressure measured inside the combustion chamber in the two tests performed. Test 1 corresponds to the segmented nozzle with the graphite nozzle insert, Test 2 to the segmented nozzle with the TaC-based throat insert. It is possible to see that when the throat insert is made of graphite the pressure after ignition decreases during the test, whereas in the other case a stable pressure value is measured when the mass flow rate is constant.

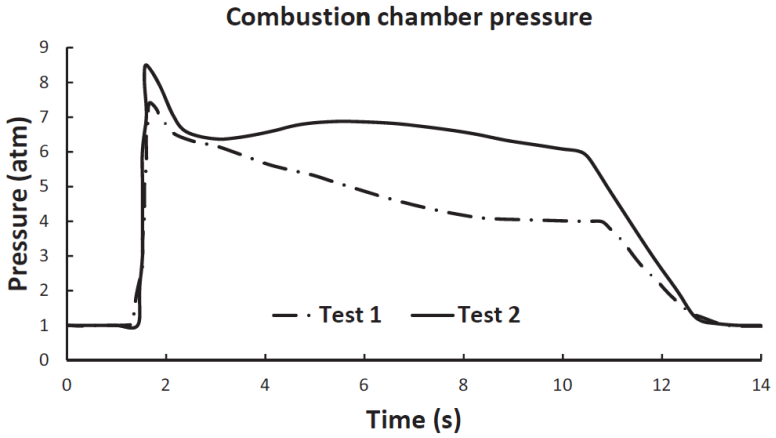

Figure 20 Chamber pressure time profile for the 3 tests [25].

The average throat erosion rate was measured evaluating the throat diameter before and after the test with a digital caliper (accuracy 60 micron) and dividing the radius variation by the test duration. During the first test with the graphite throat insert the throat was eroded due to a combination of chemical reaction and mechanical abrasion: the average erosion rate in this case was 0.28 mm/s, and this explains the sudden pressure decrease shown in Figure 20. With the TaC-based nozzle insert no ablation occurred in the throat, as shown in Figure 21a. The outer surface is unchanged after the test, the material kept its original color and no visible chemical alteration was observed, although radial cracks were observed (Figure 21b and c).The presence of the cracks demonstrates the fragility of these UHTC materials, which may be overcome by the use of fiber-based Ceramic Matrix Composites. On the other hand, a zero-erosion response is extremely interesting for propulsion applications, since a constant nozzle throat diameter allows the performances to be much more stable during the whole operating time: in fact, thrust shows a time profile similar to the one of the combustion chamber, which, as already explained, is strongly influenced by the throat section erosion.

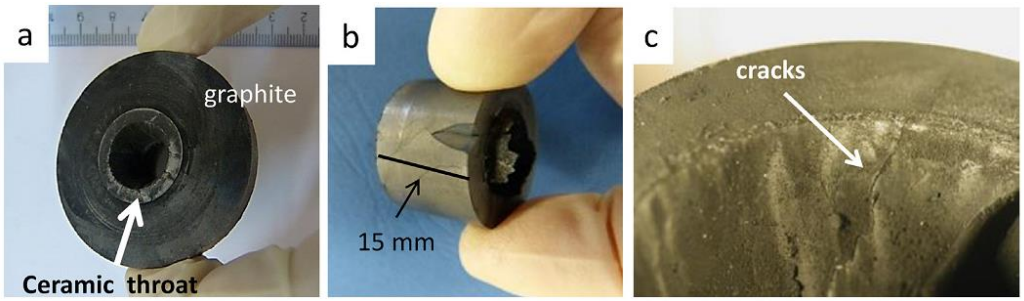

Figure 21 (a) Segmented nozzle (after removal of the converging outer element), (b) ceramic throat, (c) details of the ceramic throat showing radial cracks [25].

3.3 Numerical simulations

Besides the experimental activity, proper numerical models for the evaluation of the operating conditions and the thermo-fluid dynamic flow field inside the combustion chamber of hybrid rocket engines were developed, which have predictive capabilities and are able to provide additional information that are difficult

to collect experimentally. These models can be then coupled with the thermal analysis of the new materials samples or inserts.

A one-dimensional model based on NASA CEA software, similar to the one described in Section 2.3, can be used to rapidly evaluate both the operating conditions in the combustion chamber and through the nozzle and the performances of a hybrid rocket engine. In this case, the input of the model are the oxidizer mass flow rate, the geometrical dimensions of the fuel grain and the operating time. Given these inputs, the average fuel mass flow rate can be evaluated integrating in time the well-known regression rate law

$$\dot{r} = a\, G_{ox}^{n} \tag{1}$$

where $\dot{r}$ is the regression rate and $G_{ox} = \frac{4}{\pi}\frac{\dot{m}_{ox}}{D^2}$ the oxygen mass flux; *a* and *n* are two constants depending on the propellants combination, which can be retrieved from the data available in literature [47]. Finally, a mass balance is used to evaluate the pressure, the temperature and the chemical composition in the combustion chamber and through the nozzle and, consequently, the performances of the engine.

For more detailed analysis, a proper numerical model was implemented which allows the investigation of the internal ballistic of hybrid rockets by solving the Reynolds averaged Navier-Stokes equations for single-phase multicomponent turbulent reacting flows with variable thermodynamic and transport properties [48,49] In order to obtain predictive capabilities that allow the calculation of the fuel regression rate and the chamber pressure, the theoretical model formulation is completed by assigning the boundary conditions at the interface between the gaseous flow region and the solid fuel wall, based on the mass, energy and species balance and an Arrhenius-type equation for the fuel pyrolysis. Finally, a forward numerical integration of the local fuel regression rate was implemented in order to calculate the grid nodes displacement due to the fuel consumption during the operation time.

Figure 22 shows an example of the computational grid corresponding to the internal volume of the hybrid rocket described above, while Figure 23 shows an example of the results of the CFD model in terms of temperature contour plot, streamlines (top half) and mean mixture fraction iso-contour lines (bottom half). The model was validated comparing the numerically evaluated and the experimentally measured consumption profiles for different test [49], as shown in Figure 24.

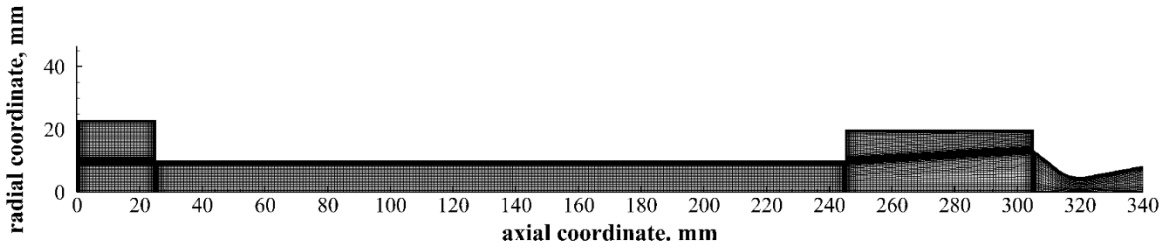

Figure 22 Typical computational grid for the simulation of Hybrid Rocket internal ballistic [48,49].

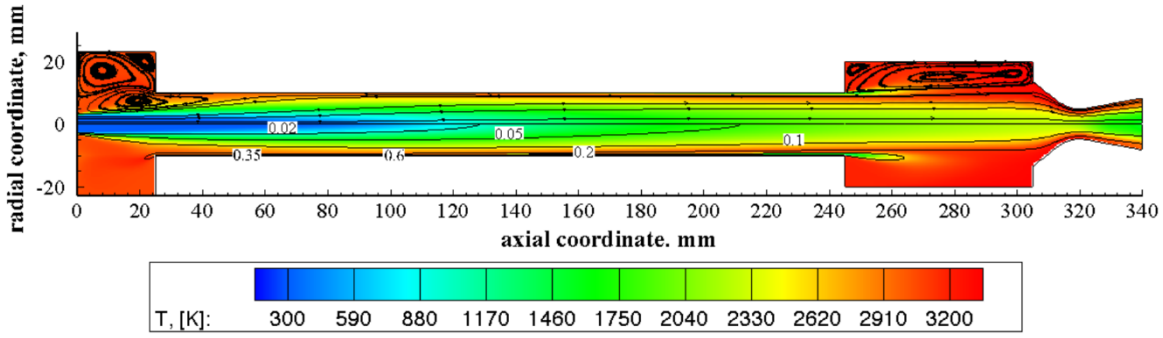

Figure 23 Temperature contour plot with overlapped streamlines (top half) and mean mixture fraction isocontour lines (bottom half) [48,49].

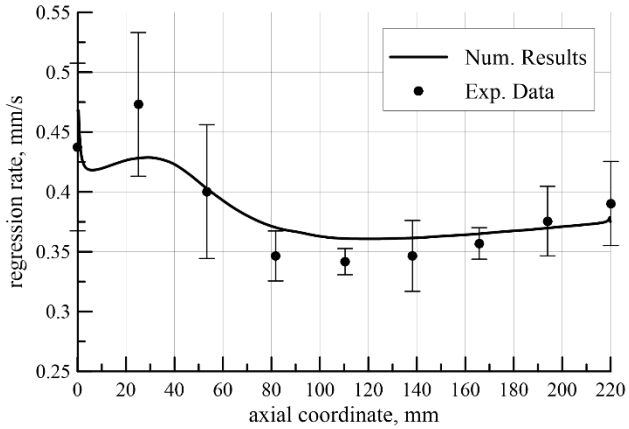

Figure 24 Comparison between measured and calculated after-burn port diameter [49].

In the framework of the current research activities, the described model can be employed in order to carry out thermal analysis of specimens or larger components.

For example, the velocity, temperature and species profile on the exit section of the nozzle can be given as input for the numerical simulation of the external exhaust plume of the engine. This analysis can be then coupled to the thermal analysis of a solid sample exposed to the hot jet for the evaluation of the heat flux on the surface and the temperature in the sample.

Finally, thermal analysis of the engine components, such as thermal protections or the nozzle, can be performed. Figure 25 shows the thermal field inside a hybrid rocket nozzle made of a ceramic material at different time during a test. The results were obtained imposing constant temperature and chemical composition at the inlet section of the nozzle. The results of the above mentioned model for the simulation of the hybrid rocket internal ballistic can be employed for the thermal analysis of the nozzle in order to achieve more accurate results. Furthermore, a model for the evaluation of the thermo-chemical erosion of the inner surface will be implemented [50].

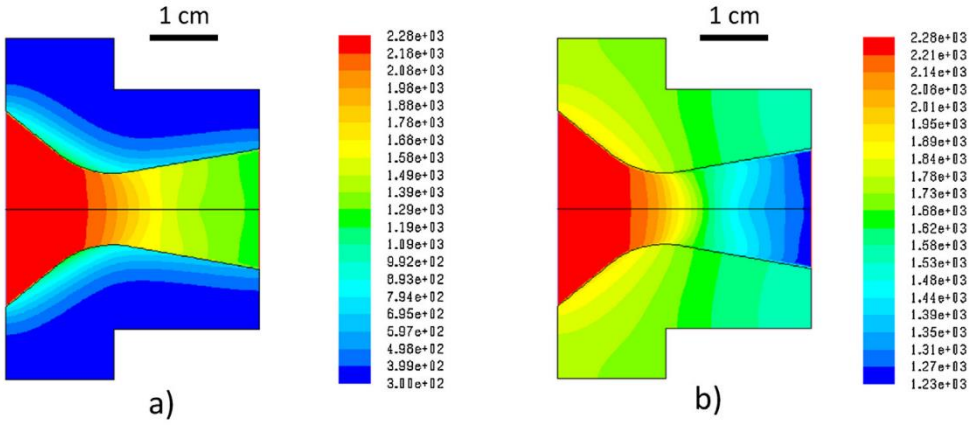

Figure 25 Computed temperature distributions (K) in the nozzle for typical operating conditions corresponding to a combustion chamber pressure of 10 bar and oxygen fuel ratio 3, after 1 s (a) and 20 s (b) from ignition.

4 Current research activities

In the framework of the European Union's Horizon2020 research and innovative program, the University of Naples "Federico II" (UNINA) is involved in C^{3}HARME research project, focused on a new class of Ultra-High-Temperature Ceramic Matrix Composites for near zero-erosion rockets nozzles and near zero-ablation thermal protection systems. The project foresees a 4-year plan of research activities, aimed at introducing innovative material solutions with high performances and optimizing standard processing techniques in order to manufacture final products suitable for space applications.

The project relies on the integration of extensive existing experience with both UHTCs (ultra-high temperature ceramics) and CMCs (ceramic matrix composites). Well-established techniques for CMC production will be integrated with state-of-art methods for the hot consolidation of ultra-refractory ceramics. In C^{3}HARME the following key technologies will be introduced:

- **Spark plasma sintering (SPS**), enabling fast thermal consolidation of UHTCMCs;
- **Microwave CVI (MCVI)**, offering excellent control over the matrix structure and degree of bonding with the fibers, thus enabling optimum fracture toughness values;
- **Reactive melt infiltration (RMI)**, a versatile technique that enables the manufacturing of dense UHTCMCs composites with dimensions up to 500 mm diameter/square and 20 mm in thickness;
- **Polymer-Infiltration & Pyrolysis (PIP)**, a well-established and robust process technique to fabricate CMC parts for propulsion and re-entry at the industrial scale.

The University of Naples "Federico II" contributes to the definition of the requirements and is responsible for the prototypes design and the identification of the corresponding testing conditions. An incremental approach proposes to start the experimental campaign with simple material samples and increasing the complexity up to a Technology Readiness Level (TRL) 6. The experimental activities are performed also in collaboration with DLR and Avio Spa in order to characterize the materials in different experimental conditions, with incremental scale up. The University of Naples "Federico II" performs tests on samples for both applications.

Arc-jet testing includes experimentation on small specimens (dimensions in the order of 1 cm), with TRL up to 4, in a relevant atmospheric re-entry environment, Figure 26(a). Characterizations allow identifying the most promising material compositions and manufacturing processes, before starting experimental activities on larger and more complex geometries (Figure 26(b),(c)), to be carried out at DLR facilities. Figure 27 shows a photo captured during test in plasma arc-jet wind tunnel at DLR facilities.

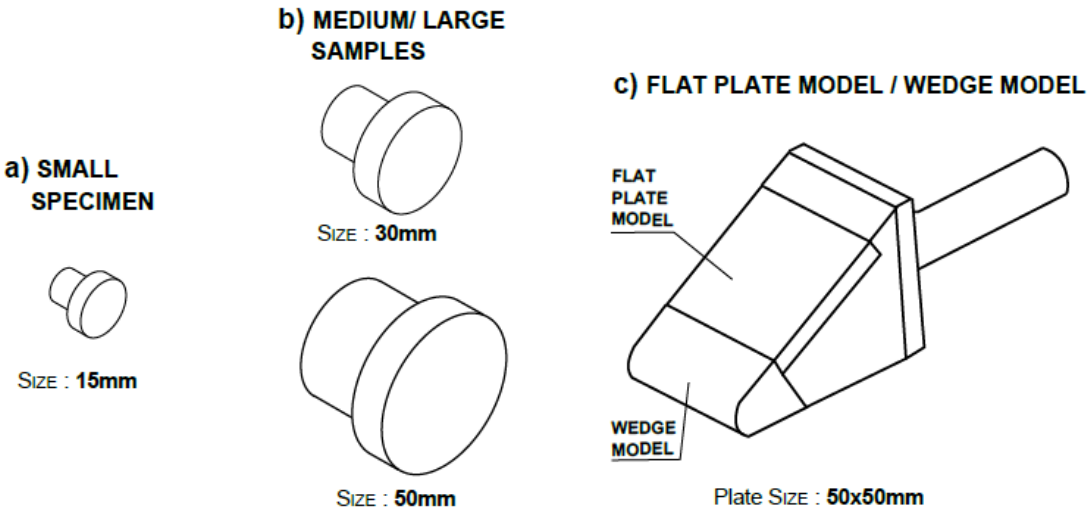

Figure 26 Design of prototypes to be tested in arc jet facilities at the University of Naples "Federico II" and DLR in C³HARME Project.

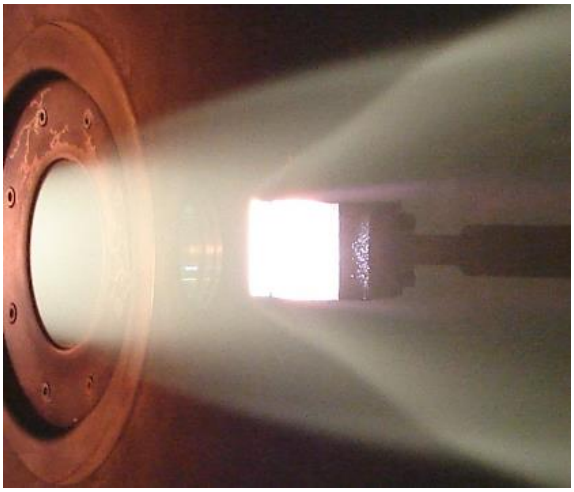

Figure 27 Test with flat plate model and wedge model in DLR arc jet plasma wind tunnel.

The reference mission for the UHTCMC thermal protection systems in the C³HARME project, defined by AIRBUS Safran Launcher, is the re-entry from Low Earth Orbit (LEO) of Advanced Re-entry Vehicle (ARV) re-entry module spacecraft. Table 3 and Table 4 show the main environmental requirements for the materials for this application. Thus, in order to use UHTCMC as a front shield TPS, it has to be able to handle the conditions given in Table 4.

Re-Entry type	Max heat flux, kW/m²	Max Pressure, kPa	Heat load, MJ/m²	Remarks
Guided	684	13	211	Guided, highest heat load
Abort	1988	45	98	Abort, highest heat flux
Abort	749	65	42	Abort, highest pressure

Table 3 Aero-thermo dynamic parameters for critical points on front shield.

Req. Id	Specification	Remark
C3HARME-ATD-01	• Maximum stagnation pressure ○ 65 kPa	From abort trajectory (ARV)
C3HARME-ATD-02	• Peak heat flux ○ 1988 kW/m^2	
C3HARME-ATD-03	• Integrated heat load ○ 211 MJ/m^2	From guided/lifting trajectory (ARV)

Table 4 Aero-thermo-dynamic requirements.

From Table 3 the critical conditions for both heat flux and pressure requirements correspond to the abort (ballistic) reentry scenario. However the materials shall not withstand simultaneously the maximum heat flux at the maximum pressure and for the maximum integrated heat load.

The facility at the University of Naples "Federico II" is not able to guarantee the maximum heat flux requirement (2 MW/m^2) and the maximum required pressure (more than 60 kPa) simultaneously. On the other hand the worst environment for UHTCMC ablation should be at the maximum heat flux and at the lowest possible pressure. In fact, under well known values of the temperature-pressure domain, SiC suffers an active oxidation with significant mass losses [51], see Figure 29. Therefore, the transition from passive to active oxidation of UHTCMCs materials based on SiC fibers takes place at the lowest pressures.

Furthermore, also for Si-free ZrB_2-based ceramic composites (e.g. with Carbon fibers) low partial pressure conditions are critical in terms of ablation behavior, since the glassy phase formed by Boron oxides is actively removed at high temperatures and low pressures. At reduced pressures significant mass losses (ablation) may occur, making this phenomenon interesting to be investigated. In conclusion it is important to test the UHTCMC samples at the largest enthalpies and at the lowest pressures to evaluate their ablation behavior.

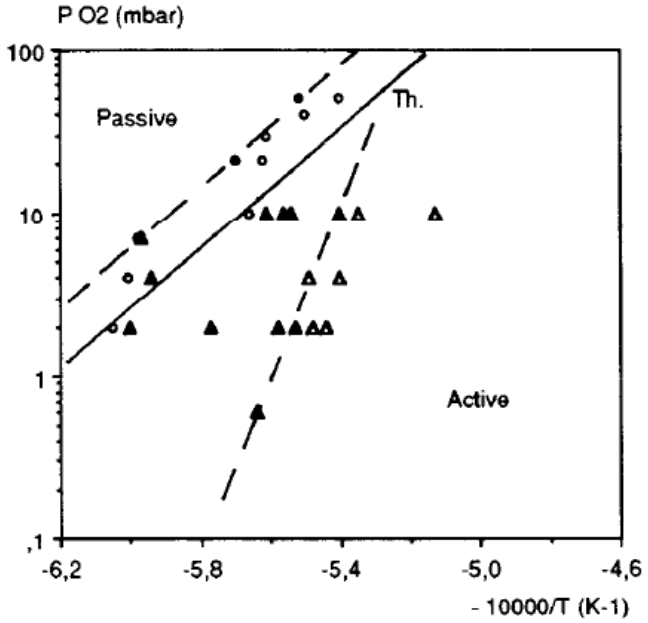

Figure 28 Oxygen partial pressure versus temperature for the active to passive transition of SiC under molecular (o) and (∆) dissociated air [51].

Tests at UNINA with the small specimens (Figure 26(a)) are performed according to the typical procedure described in Section 2.2. Table 5 summarizes the main reference test conditions for experimentation in

hypersonic arc jet facility at University of Naples “Federico II”, according to previous considerations on the environmental requirements.

Test duration	3 min
Mass Flow Rate	1 g/s
Max Specimen Temperature	2000 – 2500 K
Max Flow Total Specific Enthalpy	20 – 22 MJ/kg
Max Flow Temperature	5000 – 6000 K
Max wall total heat flux	3 – 5 MW/m^2

Table 5 Typical operative and environmental conditions in a SPES test.

A schematic of the mechanical support designed for C^{3}HARME experimental campaign is illustrated in Figure 29 . The test article (1), a flat cylinder sample (like-button), is fixed in the 100 mm-long ceramic tube insulator (2). The assembly of the sample and ceramic tube is fixed in the holder interface (3) in carbon graphite. This interface has the purpose to support the ceramic tube and thermally protect the sting support system (4) connected with screws to the interface with moving system (5) made in aluminum.

1	UHTCMC Specimen
2	Ceramic Tube Insulator (Mullite)
3	Holder Interface (Graphite)
4	Sting support System (Inconel or Steel)
5	Interface with moving system (Aluminium)

Table 6 Components of the exploded axonometric view (UNINA arc-jet tests).

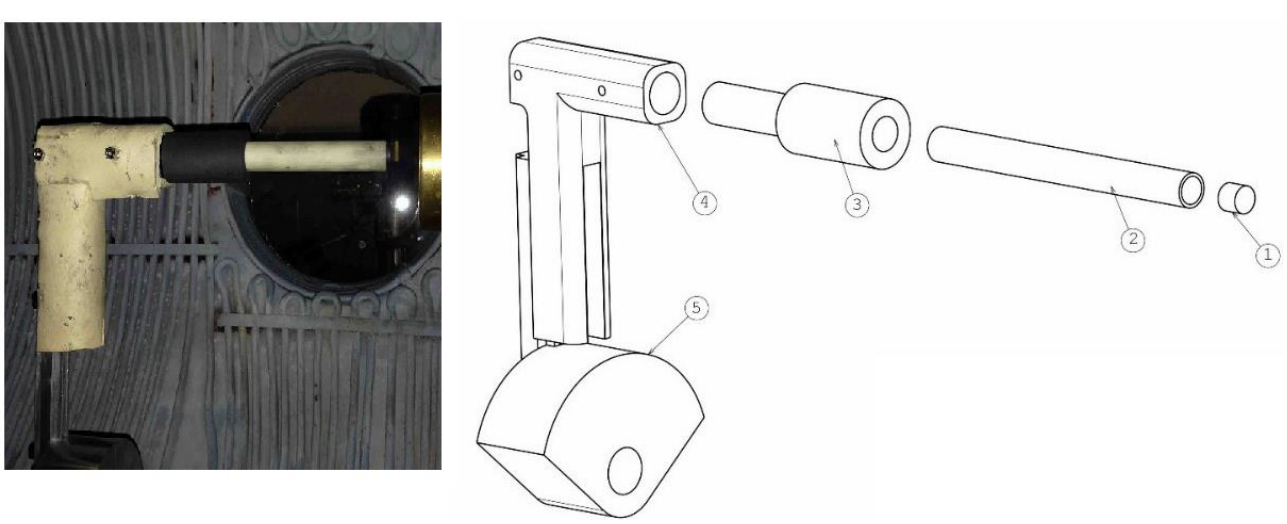

Figure 29 Mechanical support for the test article inside the test chamber of the hypersonic arc-jet facility UNINA (C³HARME Project).

In the frame of the activities on space and aerospace civil applications on UHTCMC for propulsion, Table 7 summarizes the operative conditions for Solid Rocket Motors (SRM) and Hybrid Rocket Motors (HRM).

	Range SRM	Range HRM
Pressure (bar)	50-100	5-25
Combustion time (s)	70-150	>10
Throat diameter (m)	0.1-1	0.1-0.2
Throat flame temperature (K)	≈3000 K	≈3000 K
Throat heat flux (MW/m^2)	5 - 30	5 - 15

Table 7 Rocket nozzles operative ranges.

The values of the throat flame temperature (≈3000 K), the operative pressure (50-100 bar for Solid Rocket Motors, 5-25 bar for Hybrid Rocket Motors) and throat heat flux (5-30 MW/m^2 SRM, 5-15 MW/m^2 HRM) are important parameters to identify the operative conditions in which the material must operate. For the typical propulsion applications the maximum value of operative temperature (3000 K) refers to the flame temperature, while the maximum expectable temperature of the specimen or prototype to be tested will be in the order of 2000-2500 K in the different experiments. Of course the real temperature that shall be experienced strongly depends on the capability of the material to withstand extreme conditions, without large damages and/or erosion, on the material thermal conductivity, on the test duration and on the erosion rate. Figure 30 shows the typical chemical compositions of the combustion chamber of hybrid and solid rockets in representative operating conditions.

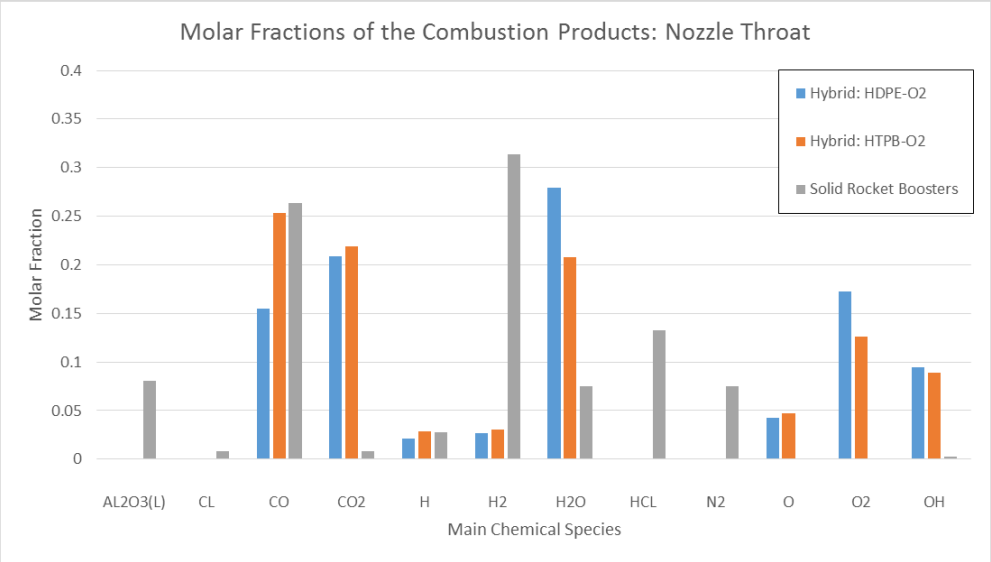

Figure 30 Molar fractions of the combustion products in rockets with different propellants.

Figure 31 shows the design of the different proposed test articles for rocket applications. Ad-hoc test setups are under development. First, free-jet tests will be performed, exposing small button-like samples (Figure 31(a)) to the exhaust plume of the rocket. The corresponding setup is shown in Figure 32 Figure 33. Then, according to the incremental approach, tests of chamber insert articles (Figure 31(b)) with dimensions in the order of 5 cm and tests with nozzle inserts (Figure 31(c)) characterized by more complex geometry will be performed. Sub-scaled complete nozzles will be tested at UNINA (Figure 31(d)) and DLR facilities. Finally tests on up-scaled nozzle will be carried out at Avio Spa in solid rocket motors.

Figure 34 shows a picture of the lab scale hybrid rocket during a preliminary configuration free jet test with a flat cylinder sample (Figure 31(a)) made of graphite.

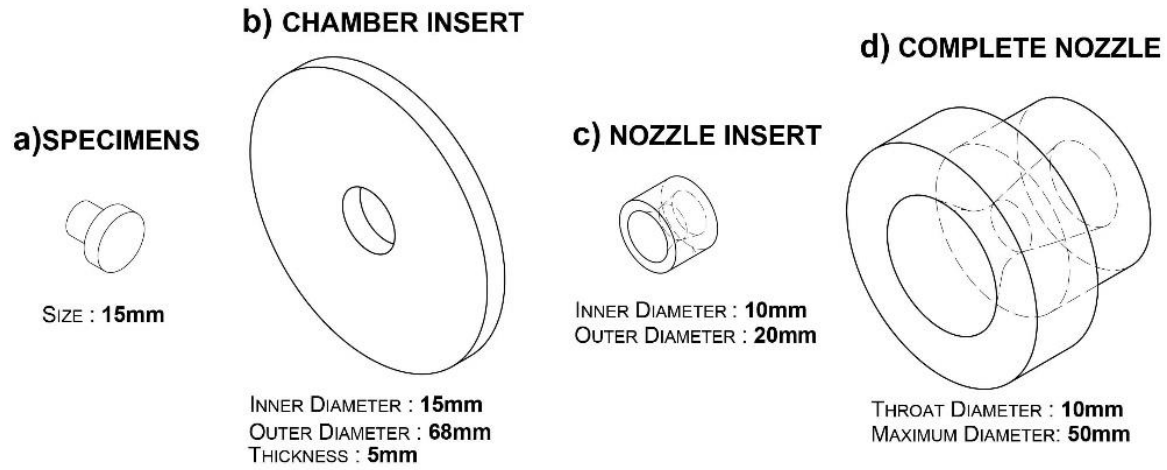

Figure 31 Design of the test articles for C³HARME experimental campaign at Hybrid Rocket Propulsion Laboratory (UNINA).

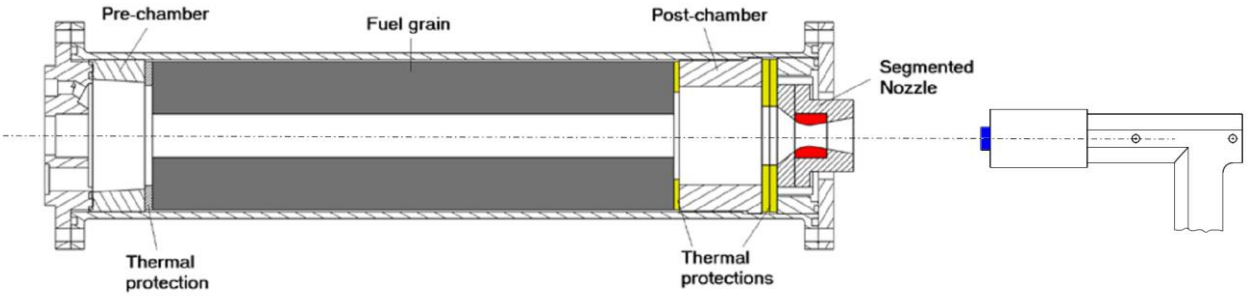

Figure 32 Schematic section of Hybrid Rocket Motors and Free jet test experimental setup with test articles:
Flat cylinder specimen (Figure 31(a)): BLUE; Chamber insert (Figure 31(b)): YELLOW; Nozzle insert (Figure 31(c)): RED.

1	UHTCMC Specimen
2	Ceramic Tube Insulator (Mullite)
3	Holder Interface (Graphite)
4	Sting support System (Inconel or Steel)
5	Interface with moving system (Aluminium)

Table 8 Components of the exploded axonometric view (Free jet tests)

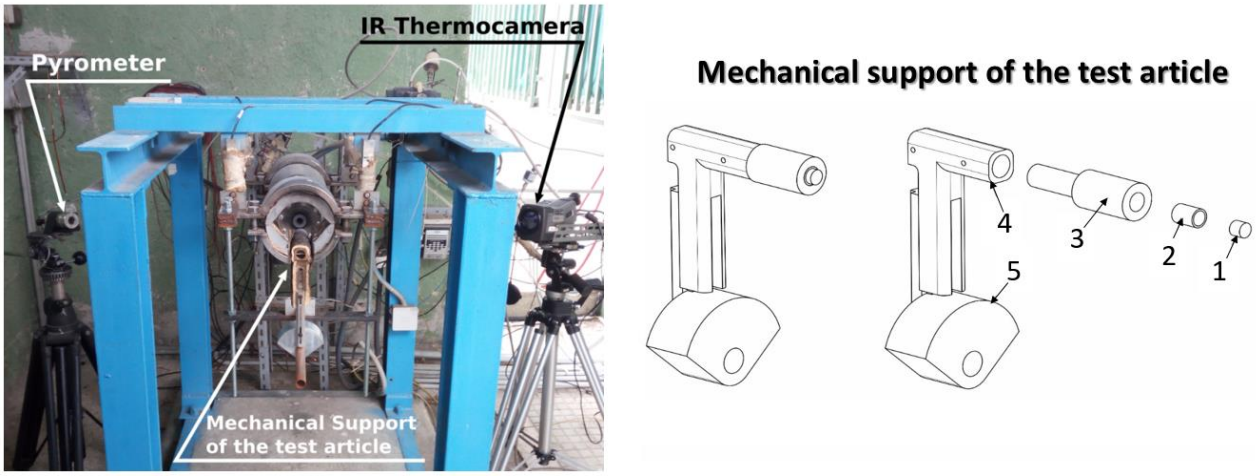

Figure 33 Free jet test experimental setup, with measurement instruments and mechanical support of the test article.

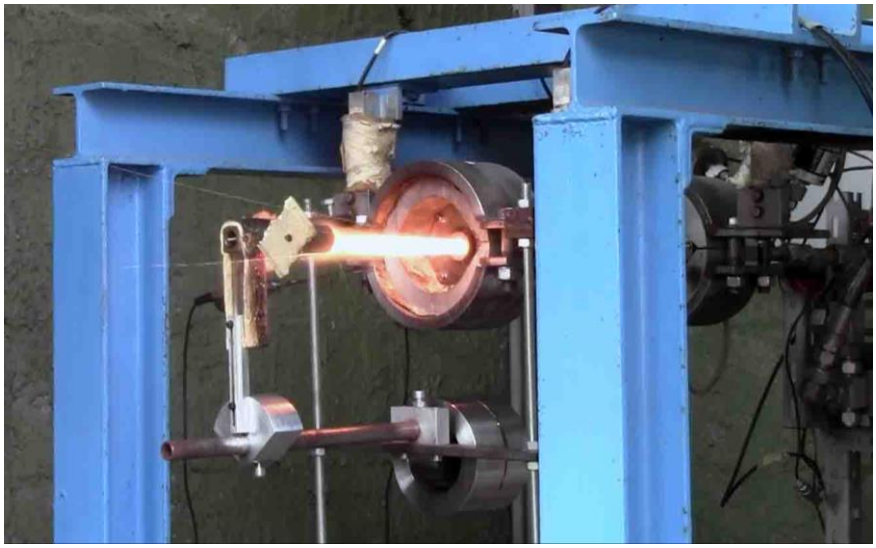

Figure 34 Preliminary Configuration Free jet test at Aerospace Propulsion Laboratory of University of Naples "Federico II".

UNINA is also responsible for activities related to numerical simulations, preliminary with respect to the test campaigns. The aim of such simulations is the evaluation of the thermo-fluid-dynamic flow-field around the test articles during the tests, for both applications.

For this purpose, the numerical models discussed in the previous sections will be improved and applied to simulate the multi-reactive flows for both hypersonic re-entry and combustion environment. In this way, it will be possible to better identify the environmental conditions in which the tests will be performed.

5 Conclusions

In this work an overview of the recent studies and of the current research programs of the University of Naples "Federico II" on Ultra-High-Temperature Ceramic (UHTC) materials was presented. These innovative materials have to withstand extremely demanding environmental conditions (high temperature, high mechanical stress, chemical reacting environment). The typical research activities include the design of prototypes for the experimental campaigns, tests on samples in both re-entry and combustion environments, numerical modelling and simulations of reacting flows onto the test article surfaces.

To investigate the typical materials behavior in atmospheric re-entry conditions, relevant tests are carried out with an arc-jet facility, with a maximum specific total enthalpy higher than 20 MJ/kg, supersonic Mach number and temperatures higher than 2000 K in a gas atmosphere of highly dissociated oxygen. Samples with different dimensions and shapes were tested to simulate the conditions reached at the stagnation point of a re-entry vehicle, with flat or hemispherical specimens, or leading edges, with the wedge shape. Pyrometry and thermography techniques allow to measure temperature on the samples while the microstructures of the tested samples are analyzed thanks to a collaborative partnership with ISTEC. The most promising materials are characterized by a layered multiphase configurations of oxide scales protecting the unoxidized core substrates.

On the other hand, the Aerospace Propulsion Laboratory, which is mainly conceived for testing of hybrid rockets, allows the characterization of materials under extreme conditions representative of propulsion environment. In particular, the behavior of a segmented nozzle with a ceramic throat insert is investigated.

For both the mentioned applications, the experimental activities are supported by numerical simulations that become a viable and largely recommended tool not only to predict the thermo-chemical evolution of the gas but also to characterize the flow-field surrounding the proof article inside the testing chamber. For these purposes, CFD models for the simulation of the multicomponent turbulent reacting flows either in the SPES

arc-jet facility or in the hybrid rocket combustion chamber are proposed and properly validated. Finally, thermal analyses of the materials samples are performed.

The current research activities in the framework of the C^{3}HARME research project are focused on a new class of Ultra-High-Temperature Ceramic Matrix Composites (UHTCMC) for near zero-erosion rockets nozzles and near zero-ablation thermal protection systems. Following an incremental approach, different kinds of UHTCMC samples are designed, in order to perform characterization tests for both hypersonic re-entry and rocket propulsion applications. Numerical simulations, based on the models described in this work, support the experimental activities.

6 Acknowledgements

The C^{3}HARME research project has received funding by the European Union's Horizon2020 research and innovation programme under the Grant Agreement 685594.

References

[1] G.J.K. Harrington, G.E. Hilmas, "Thermal conductivity of ZrB_2 and HfB_2", in: W. Fahrenholtz, E. Wuchina, W. Lee and Y. Zhou, "Ultra-High Temperature Ceramics: Materials for Extreme Environment Applications", 1st ed., John Wiley & Sons, Inc., 2014, pp. 197-235.

[2] E. Eakins, D.D. Jayaseelan, W.E. Lee, "Toward Oxidation-Resistant ZrB_2-SiC Ultra High Temperature Ceramics", *Metallurgical and Materials Transactions A* 42 (4), 878-887 (2011).

[3] M. Natali, J.M. Kenny, L. Torre, "Science and technology of polymeric ablative materials for thermal protection systems and propulsion devices: A review," *Progress in Materials Science* 84, 192-275 (2016).

[4] T.A. Parthasarathy, D. Petry, M.K. Cinibulk, T. Mathur, M.R. Mark, R. Gruber, "Thermal and Oxidation Response of UHTC Leading Edge Samples Exposed to Simulated Hypersonic Flight Conditions", *Journal of the American Ceramic Society* 96 (3), 907-915 (2013).

[5] G. P. Sutton, O. Biblarz, *Rocket Propulsion Elements*, 7th ed., New York: Wiley and sons, 2001.

[6] P. Thakre, V.Yang , "Chemical erosion of carbon-carbon/graphite nozzles in solid-propellant rocket motors," *Journal of Propulsion and Power* 24 (4) 822-833 (2008).

[7] S. Tang S, Hu C. Design, Preparation and Properties of Carbon Fiber Reinforced Ultra-High Temperature Ceramic Composites for Aerospace Applications: A Review. J Mater Sci Technol. 2017;33(2):117-130.

[8] L. Galfetti, F. Nasuti, D. Pastrone, A. Russo, "An Italian network to improve hybrid rocket performance: Strategy and results," *Acta Astronautica* 96, 246-260 (2014).

[9] P. Sanoj, B. Kandasubramanian, "Hybrid Carbon-Carbon Ablative Composites for Thermal Protection in Aerospace," *Journal of Composites* 2014 (2014).

[10] J. Zheng, H. Cui, H. Lib, Y. Li, D. Yao, Z. Ying, H. Deng, "Mechanical and ablative properties of C/C composites modified by SiC using liquid silicon infiltration method", *68th International Astronautical Congress*, Adelaide, Australia, September 2017.

[11] L. Luo, Y. Wang, L. Duan, L. Liu, G. Wang, “Ablation behavior of C/SiC-HfC composites in the plasma wind tunnel”, *Journal of the European Ceramic Society* 36 (15), 3801-3807 (2016).

[12] Y. Wang, Z. Chen, S. Yu, "Ablation behaviour and mechanism of C/SiC Composites", *Journal of materials research and technology* 5, 170-182 (2016).

[13] C. Li, K. Li, H. Li, H. Ouyang, Y. Zhang, L. Guo, "Mechanical and thermophysical properties of carbon-carbon composites with hafnium carbide," *Ceramics International* 39, 6769–6776 (2013).

[14] A. Nisar, S. Ariharan, T. Venkateswaran, N. Sreenivas, K. Balani, “Oxidation studies on TaC based ultra-high temperature ceramic composites under plasma arc jet exposure”, *Corrosion Science* 109, 50-61 (2016).

[15] W.E. Lee, E. Eakins, H. Jackson, D. Jayaseelan, "Advanced characterization of composite ultra high temperature ceramic systems", in: W. Fahrenholtz, W. Lee, E.J. Wuchina, Y. Zhou, "Ultra-High Temperature Ceramics: Materials For Extreme Environmental Applications II", Aerospace Research Institute Eds, ECI Symposium Series, 2013. http://dc.engconfintl.org/uhtc/20

[16] L. Scatteia, D. Alfano, S. Cantoni, F. Monteverde, A. Di Maso, M. De Stefano Fumo, "Plasma Torch Test of an Ultra-High-Temperature Ceramics Nose Cone Demonstrator", *Journal of Spacecraft and Rockets* 47 (2), 271-279 (2010).

[17] A. Paul, J.G.P. Binner, B. Vaidhyanathan, A.C.J. Heaton, P.M. Brown, “Oxyacetylene torch testing and microstructural characterization of tantalum carbide”, *Journal of Microscopy* 250 (2) 122-129 (2013).

[18] M. Natali, M. Monti, J.M. Kenny, L. Torre, “A nanostructured ablative bulk molding compound: Development and characterization”, *Composites Part A: Applied Science and Manufacturing* 42 (9), 1197-1204 (2011).

[19] L. Pienti, D. Sciti, L. Silvestroni, A. Cecere, R.Savino, “Ablation tests on HfC- and TaC-based ceramics for aeropropulsive applications”, *Journal of the European Ceramic Society* 35, 1401-1411 (2015).

[20] D. Sciti, L. Zoli, L. Silvestroni, A. Cecere, G.D. Martino, R.Savino, "Design, fabrication and high velocity oxy-fuel torch tests of a Cf-ZrB_2- fiber nozzle to evaluate its potential in rocket motors," *Materials and Design* 109, 709-717 (2016).

[21] A. Cecere, R. Savino, C. Allouis and F. Monteverde, "Heat transfer in ultra-high temperature advanced ceramics under high enthalpy arc-jet conditions," *International Journal of Heat and Mass Transfer* 91, 747-755 (2015).

[22] F. Monteverde, R. Savino, “ZrB_2–SiC sharp leading edges in high enthalpy supersonic flows”, *Journal of the American Ceramic Society* 95 (7), 2282-2289 (2012).

[23] R. Savino, M. De Stefano Fumo, L. Silvestroni, D. Sciti, "Arc-jet testing on HfB_2 and HfC-based ultra-high temperature ceramic materials," *Journal of the European Ceramic Society* 28, 1899–1907 (2008).

[24] F. Monteverde, R. Savino, M. De Stefano Fumo, "Dynamic oxidation of ultra-high temperature ZrB2–SiC under high enthalpy supersonic flows," *Corrosion Science* 53, 922-929 (2011).

[25] R. Savino, G. Festa, A. Cecere, L. Pienti, D. Sciti., "Experimental set up for characterization of carbide-based materials in propulsion environment.," *Journal of the European Ceramic Society* 35, 1715-1723 (2015).

[26] M. Tausche, R. Janovsky, M. Scheper, J. Apeldoorn, R. Monti, R. Savino, M. De Stefano Fumo, D. Paterna, E. Di Sotto, J. Branco, "PHOEBUS: a high lift-over-drag vehicle for re-entry", *60th International Astronautical Conference*, Daejeon, Republic of Korea, 2-16 October 2009.

[27] R. Savino, G. Russo, V. Carandente, V. D'oriano, "Hyplane for Space Tourism and Business Transportation", *Journal of the British Interplanetary Society* 62 (2), 82-89 (2014).

[28] R. Savino, G. Russo, V. Carandente, V. D'Oriano, "Hyplane: Challenges for Space Tourism and Business Transportation", Journal of Aeronautics & Aerospace Engineering 2 (5) (2013), http://dx.doi.org/10.4172/2168-9792.1000123.

[29] E. Trifoni, R. Savino, A. Esposito, G. Tumino, "Share, Plasma Jet Impingement Tests of ESA IXV TPS Interfaces", *8th European Workshop on Thermal Protection Systems and Hot Structures*, Noordwijk, Netherlands, 19-22 April 2016.

[30] V. Carandente, G. Zuppardi, R. Savino, "Aerothermodynamic and stability analyses of a deployable re-entry capsule", *Acta Astronautica* 93, 291-303 (2013).

[31] R. Savino, V. Carandente, "Aerothermodynamic and feasibility study of a deployable aerobraking re-entry capsule", *FDMP: Fluid Dynamics & Materials Processing* 8 (4), 453-476 (2012).

[32] R. Savino, R. Aurigemma, V. Carandente, L. Gramiccia, J. Longo, L. Marraffa, F. Punzo, "Study and Development of a Sub-Orbital Reentry Demonstrator", *Journal of the British Interplanetary Society* 62 (2), 74-81 (2014).

[33] M. Iacovazzo, R. Savino, G. Zuppardi, V. Carandente, "Longitudinal stability analysis of a suborbital re-entry demonstrator for a deployable capsule", *Acta Astronautica* 106, 101-110 (2015).

[34] F. Monteverde, A. Cecere, R. Savino, "Thermo-chemical surface instabilities of SiC-ZrB_2 ceramics in high enthalpy dissociated supersonic air flows," *Journal of the European Ceramic Society* 37 (6), 2325-2341 (2017).

[35] R. Savino, M. De Stefano Fumo, D. Paterna, A. Di Maso, "Arc-Jet Testing of Ultra-High-Temperature-Ceramics", *The Open Aerospace Engineering Journal* 3, 20-31 (2010).

[36] F. Monteverde, D. Alfano, R. Savino, "Effects of LaB_6 addition on arc-jet convectively heated SiC-containing ZrB_2-based ultra-high temperature ceramics in high enthalpy supersonic airflows," *Corrosion Science* 75, 443-453 (2013).

[37] R. Savino, M. De Stefano Fumo, D. Paterna, A. Di Maso , F. Monteverde, "Arc-jet testing of ultra-high-temperature-ceramics," *Aerospace Science and Technology* 14, 178–187 (2010).

[38] A. Di Maso, R. Savino, M. De Stefano Fumo, L. Silvestroni, D. Sciti, "Arc-Jet Testing on HfB_2 - $TaSi_2$ Models: Effect of the Geometry on the on the aerothermal behaviour," *The Open Aerospace Engineering Journal* 3, 10-19, (2010).

[39] D. Sciti, R. Savino, L. Silvestroni, "Aerothermal behaviour of a SiC fibre-reinforced ZrB_2 sharp component in supersonic regime," *Journal of the European Ceramic Society* 32, 1837-1845 (2012).

[40] W. Zhang, C. Xie, M. Ge, X. Wei, “C/C-ZrB2-ZrC-SiC derived from polymeric precursor infiltration and pyrolysis”, in: I.M. Low, Y. Sakka, C.F. Hu, “MAX Phases and Ultra-High Temperature Ceramics for Extreme Environments”, IGI Global, USA, 2013, pp. 436-456.

[41] F. Monteverde, R. Savino, “Stability of ultra-high-temperature ZrB_2–SiC ceramics under simulated atmospheric re-entry conditions”, *Journal of the European Ceramic Society* 27, 4797-4805 (2007).

[42] J. Marschall, D.A. Pejakovic, W.G. Fahrenholtz, G.E. Hilmas, F. Panerai, O. Chazot, “Temperature Jump Phenomenon During Plasmatron Testing of ZrB_2-SiC Ultrahigh-Temperature Ceramics”, *Journal of Thermophysics and Heat Transfer* 26, 569-572 (2012).

[43] F. Panerai, B. Helber, O. Chazot, M. Balat-Pichelin, “Surface temperature jump beyond active oxidation of carbon/silicon carbide composites in extreme aerothermal conditions”, *Carbon* 71, 102-119 (2014).

[44] S. Gordon, B.J. McBride, “Computer Program of Complex Chemical Equilibrium Compositions and Applications”, NASA Reference Publication 1311, 1994.

[45] D. Sciti, L. Silvestroni, S. Guicciardi, D. Dalle Fabbriche, A. Bellosi, “Processing, mechanical properties and oxidation behavior of TaC and HfC composites containing 15 vol% $TaSi_2$ or $MoSi_2$”, *Journal of Material Research* 24 (6), 2056–2065 (2009).

[46] J.W. Zimmermann, G.E. Hilmas, W.G. Fahrenholtz, “Thermal shock resistance of ZrB_2 and ZrB_2-30% SiC”, *Materials Chemistry and Physics* 112 (1), 140-145 (2008).

[47] G. Zilliac, M.A. Karabeyoglu, “Hybrid Rocket Fuel Regression Rate Data and Modeling”, *42nd AIAA/ASME/SAE/ASEE Joint Propulsion Conference & Exhibit,* AIAA2006-4504, Sacramento, California, 2006.

[48] G.D. Di Martino, P. Malgieri, C. Carmicino, R. Savino “A Simplified Computational Fluid-Dynamic Approach to the Oxidizer Injector Design in Hybrid Rockets,” *Acta Astronautica* 129, 8-21 (2016).

[49] G.D. Di Martino, C. Carmicino, R. Savino “Transient computational thermo-fluid-dynamic simulation of hybrid rockets internal ballistics,” *Journal of Propulsion and Power*, March 2017, doi:10.2514/1.B36425.

[50] D. Bianchi, F. Nasuti, “Carbon-Carbon Nozzle Erosion and Shape Change in Full-Scale Solid-Rocket Motors,” *Journal of Propulsion and Power* 28, 820-830 (2012).

[51] M.J.H. Balat, "Determination of Active-to-Passive Transition in the Oxidation of Silicon Carbide in Standard and Microwave-Excited Air," *Journal of European Ceramic Society* 16, 55-62 (1996).